[1]Appawala Jayanthi
[2]B. Eswara Reddy

Advanced Deep Learning Techniques for Lung Cancer Diagnosis: The VDSFusion-Net Approach

Journal of Electrical Systems

Abstract: - This paper introduces an innovative approach for identifying and categorizing lung cancer using the VDSFusion-Net model, which merges VGG16 and DenseNet121 with an SVM classifier. The suggested method entails a meticulous preprocessing pipeline, which encompasses edge-directed interpolation, Wiener filtering, and CLAHE. This is then followed by segmentation utilizing Kapur's thresholding and morphological processing. The utilization of RANSAC in circle detection enhances the precision of tumor identification. The VDSFusion-Net model utilizes sophisticated methods for extracting features and classifying data, resulting in exceptional performance metrics: an accuracy of 99.32%, sensitivity of 99.45%, and specificity of 99.7%. The VDSFusion-Net model demonstrates its usefulness and uniqueness in accurately classifying lung cancer, providing substantial enhancements in diagnostic accuracy and reliability.

Keywords: *Deep Learning, Fusion, Accuracy, Lung cancer, Specificity, Sensitivity, Enhancement*.

I. INTRODUCTION

Lung cancer is a highly common and lethal type of cancer that is responsible for a substantial number of cancer-related fatalities on a global scale [1-3]. The main source of this condition is the epithelial cells that line the lungs [4-6]. Prompt identification and precise categorization of lung cancer are essential for optimal therapy and enhanced patient survival rates [7-9].

The health hazards linked to lung cancer are significant, considering its highly aggressive nature and the possibility of early metastases. Common risk factors encompass smoking, secondhand smoke exposure, radon gas, asbestos, and other environmental contaminants [10-12]. Both genetic predisposition and a previous history of respiratory disorders are additional factors that increase the risk [13]. The elevated fatality rate of lung cancer frequently arises from delayed detection, wherein the illness has already progressed to a point that restricts therapeutic alternatives [14-16]. Hence, an early and accurate diagnosis is crucial in enhancing patient outcomes and alleviating the overall burden of this illness [17].

The progress made in medical imaging and machine learning has greatly improved the capacity to identify and categorize lung cancer [18]. The deep learning models have demonstrated significant potential in evaluating intricate medical images and detecting tiny patterns that may suggest the presence of cancer [19]. These methods provide superior accuracy and reliability in comparison to conventional diagnostic techniques, allowing for earlier detection and more exact classification [20]. The integration of deep learning with medical imaging has the potential to revolutionize the diagnostic process, resulting in improved prognosis and individualized treatment strategies.

This study enhances the field by introducing the VDSFusion-Net model, which integrates VGG16 and DenseNet121 with an SVM classifier to enhance the identification and categorization of lung cancer. The methodology incorporates sophisticated preprocessing techniques such as edge-directed interpolation, Wiener filtering, CLAHE, Kapur's thresholding, and morphological processing. This is followed by circle recognition using RANSAC. In addition, the study examines the possibility of combining the VDSFusion-Net model with clinical data streams to provide real-time diagnostic assistance and thorough patient evaluation.

The organization of this paper is as follows: Section 2 examines previous research. Section 3 provides a comprehensive explanation of the suggested methodology, encompassing data pre-treatment, model architecture, and classification algorithms. Section 4 provides an overview of the experimental setup, describes the dataset used, and outlines the assessment measures and results explained with metrics Section 5 serves as the final part of the study, providing a summary and suggesting areas for future research. It highlights the need of incorporating clinical data streams to enhance diagnosis accuracy and assist healthcare professionals..

[1] *Corresponding author: Research Scholar, CSE Department, JNT University Anantapur (JNTUA), Ananthapuramu, A.P, 515002, India, email: ajayanthijntua@gmail.com
[2] Professor, CSE Department, JNT University Anantapur (JNTUA), Ananthapuramu, A.P, 515002, India

II. LITERATURE SURVEY

In 2024, Swain et al. [20] suggested utilizing the Inception v3 network for the purpose of detecting lung cancer. The study showcased remarkable performance numbers, as the network achieved a sensitivity of 96.66%, a specificity of 99.12%, and an overall accuracy of 98.29%. The results emphasize the Inception v3 network's capacity to precisely differentiate between malignant and benign lung nodules, establishing it as a dependable instrument for early lung cancer detection. Nevertheless, this strategy may be hindered by its demanding computational complexity and the requirement for high-performance technology, which may not be easily accessible in all clinical environments. This criteria may have limited relevance in contexts with limited resources.

In 2024, Kim and colleagues [21] proposed using the ImageNet pre-trained EfficientNet-B2 architecture for the purpose of detecting lung cancer. The results obtained from this method showed a sensitivity of 76.3%, a specificity of 75.0%, and an accuracy of 68.0%. Although the EfficientNet-B2 model has the benefit of being pre-trained on a large dataset, which makes transfer learning easier, its performance metrics suggest that there is still potential for improvement, particularly in terms of accuracy. A drawback of this approach is that its poorer specificity and accuracy may result in a higher incidence of false positives and false negatives, thereby impacting clinical decision-making. Additionally, the model's modest complexity may not fully use the intricacies included in medical imaging data when compared to more sophisticated architectures.

In 2024, Zhang et al. [22] conducted a study on the use of DenseNet for detecting lung cancer. The study achieved a remarkable accuracy rate of 99%, with a sensitivity of 99.3% and a specificity of 99.6%. The architecture of DenseNet is characterized by its dense connectivity between layers, which facilitates the transmission of features. Although the model has certain advantages, such as its strengths, it is important to note that it also has limits. These drawbacks include the high computing requirements and the possibility for overfitting due to the complexity of the model. These constraints are especially relevant when the model is used to smaller or less diverse datasets. The need for significant computational resources may impede its implementation in certain therapeutic environments.

In 2024, Sangeetha and colleagues [23] introduced a Multimodal Fusion Deep Neural Network, which integrates many data kinds to improve diagnostic precision. The network demonstrated an accuracy of 87.4%, a recall rate of 86.4%, and a specificity of 88%. By integrating several data modalities, a more thorough analysis may be conducted, which has the potential to enhance diagnostic outcomes. Nevertheless, the intricacy of overseeing and incorporating many data sources may provide a difficulty, and the relatively lower precision in comparison to other models implies that there is still potential for enhancement in the fusion process. Moreover, the need for various forms of data can complicate the implementation procedure.

In 2023, Rashmi et al. [24] proposed a streamlined deep neural network that aims to decrease processing demands without compromising diagnostic accuracy. The network attained an accuracy rate of 85.21%, with a sensitivity rate of 83.8% and a specificity rate of 87.7%. This lightweight methodology renders it appropriate for settings with restricted computational capacity, hence enabling wider accessibility. Nevertheless, the balance between decreased computing burden and diagnostic precision implies that this approach might not encompass all the nuanced nuances found in lung cancer imaging, perhaps resulting in less precise diagnosis in certain instances.

In 2022, Shimazaki et al. [25] employed conventional deep learning methods to diagnose lung cancer. Although these technologies have played a crucial role in enhancing medical imaging analysis, they often provide only moderate levels of accuracy and sensitivity. The main drawback of conventional deep learning techniques is their dependence on extensive labeled data and significant computational resources, which might be a challenge in clinical environments with limited data and processing capacities.

In 2022, Wang et al. [26] utilized fundamental deep learning methods to analyze the LIDC dataset in order to diagnose lung cancer. This approach offers a fundamental level of performance, which is valuable for the purpose of making comparisons. Nevertheless, fundamental deep learning techniques sometimes encounter difficulties when dealing with intricate patterns in medical pictures and may fail to attain the level of accuracy necessary for dependable clinical applications. These models have disadvantages such as a propensity to overfit on limited datasets and a requirement for substantial processing resources.

In 2022, Salama et al. [27] utilized deep generative models to identify lung cancer, reaching an overall detection accuracy of 98.91%, with a sensitivity of 98.46% and a specificity of 97.72%. Deep generative models are highly effective in creating artificial data and enhancing the resilience of detection systems. Nevertheless, the intricacy of these systems and the need for a substantial amount of training data might pose considerable constraints. Moreover,

the comprehensibility of generative models might pose a challenge, rendering the decision-making process in medical diagnostics hard to grasp, a vital aspect.

III. PROPOSED SYSTEM

The process begins with the loading of an image from the LIDC-IDRI dataset [10] in the first stage of the proposed methodology, which is depicted by a block diagram in Figure 1.The process begins by scaling the input image using edge-directed interpolation and applying Wiener filtering to reduce noise. CLAHE is then used to enhance the image, followed by Kapur's thresholding for binary conversion. Morphological processing (erosion and dilation) cleans up the image, and inverted binary images are created for active contour segmentation. Circles are detected using RANSAC, and the tumor area is measured. The VDSFusion-Net model, combining VGG16, DenseNet121, and an SVM classifier, is used to classify the tumor areas. Finally, the outcomes are displayed with segmented areas and tumor metrics superimposed on the original image.

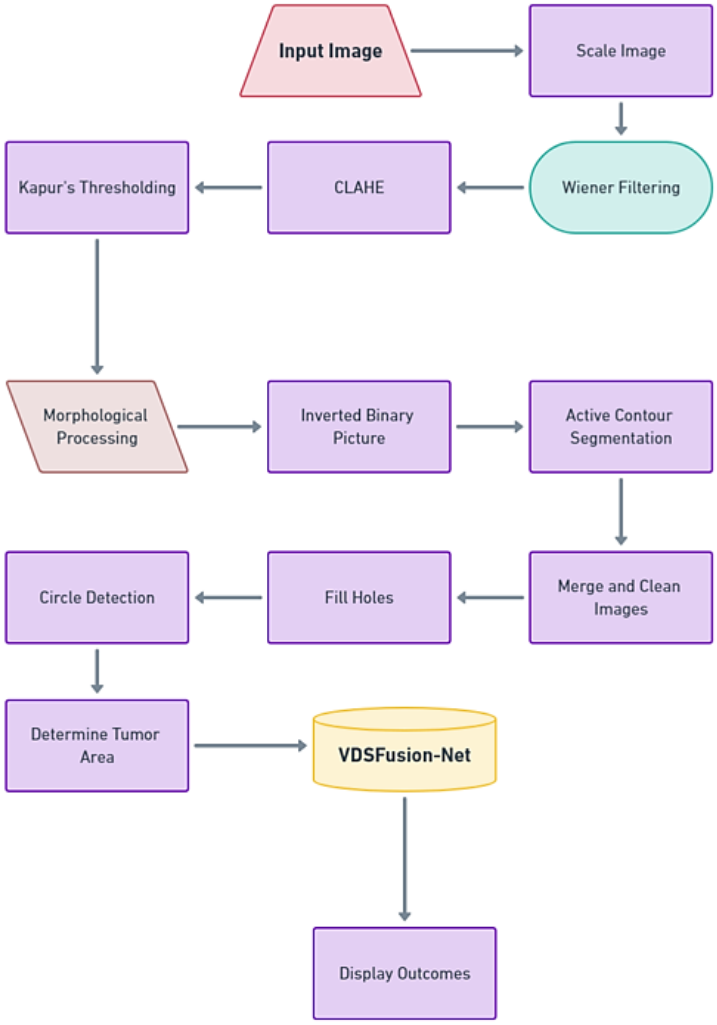

Fig. 1 Proposed Block Diagram for Lung Cancer Detection

Now the entire process of the proposed system is explained in elaborate form below.

The methodology for lung cancer detection starts by scaling the input image using edge-directed interpolation. This method maintains the clarity and intricacy of boundaries, guaranteeing the preservation of crucial characteristics while adjusting the size, which is important for precise medical picture examination.

First, we begin by scaling the input image f(x, y) using edge-directed interpolation to obtain an interpolated image $f_{interp}(x', y')$. If S is the scaling factor, the new coordinates (x', y') are computed as:

$x' = S.x$.....(1)

$y' = S.y$.....(2)

Afterwards, Wiener filtering is utilized to decrease noise while maintaining image details. The Wiener filter, unlike median filtering, adjusts to the local picture variance, providing better noise reduction.

The Wiener filter adapts to the local image variance, and the filtered image $f_{wiener}(x, y)$ is given by:

$$f_{wiener}(x,y) = \mu_f(x,y) + \frac{\sigma_f^2(x,y) - \sigma_n^2}{\sigma_f^2(x,y)}(f(x,y) - \mu_f(x,y)) \quad \ldots\ldots(3)$$

where $\mu_f(x,y)$is the local mean, $\sigma_f^2(x,y)$ is the local variance, and σ_n^2 is the noise variance.

In order to improve the image, CLAHE is employed. This technique evenly distributes the intensity of light throughout the image, resulting in enhanced visibility of minute features. This is particularly important in medical imaging as it helps to highlight subtle differences.

If P(I) is the pixel intensity probability function, the CLAHE-enhanced image $f_{CLACHE}(x, y)$ is:

$$f_{CLACHE}(x,y) = \frac{cdf(f(x,y)) - cdf_{min}}{1 - cdf_{min}} * (L\text{-}1) \quad \ldots\ldots(4)$$

where cdf is the cumulative distribution function of pixel intensities, cdf_{min} is the minimum non-zero value of the cdf, and L is the number of possible intensity levels.

Subsequently, the improved image is transformed into a binary format via Kapur's thresholding technique. This method calculates the ideal threshold value by maximizing the entropy between the segmented sections, guaranteeing a successful differentiation between the foreground and background. Kapur's approach is highly beneficial for medical imaging since it effectively employs histogram information to achieve accurate segmentation.

The optimal threshold T is calculated by maximizing the sum of entropies of the foreground and background regions:

$$T = arg\ max_t[H(B_t) + H(W_t)] \quad \ldots\ldots(5)$$

where H(Bt) and H(Wt) are the entropies of the background and foreground regions at threshold t, defined as:

$$H(B_t) = -\sum_{i=0}^{t} P(i) \log P(i) \quad \ldots\ldots(6)$$

$$H(W_t) = -\sum_{i=t+1}^{L-1} P(i) \log P(i) \quad \ldots\ldots(7)$$

with P(i) being the probability of intensity level i.

Next, the binary picture is subjected to morphological processes, first with erosion and then followed by dilation (known as morphological opening) in order to eliminate minor noise and create smoother object boundaries. The segmentation is further refined by repeating this process with a different organizing element.

The erosion and dilation operations are defined as:

$$(f \ominus S_E)(x,y) = \min_{(i,j)\in S_E} f(x+i,\ y+j) \quad \ldots\ldots(8)$$

$$(f \oplus S_E)(x,y) = \max_{(i,j)\in S_E} f(x-i,\ y-j) \quad \ldots\ldots(9)$$

The morphological opening operation $f_{opened}(x, y)$ is:

$$f_{opened}(x,y) = (f \ominus S_E) \oplus S_E \quad \ldots\ldots(10)$$

This process is repeated with a different structuring element S_{E2} for further refinement:

$$f_{opened2}(x,y) = (f_{opened} \ominus S_{E2}) \oplus S_{E2} \quad \ldots\ldots(11)$$

To make an inverted binary picture, all pixel values are set to 1 and then the morphologically opened image is subtracted from this inverted image. This process is iterated to produce two distinct inverted binary pictures for subsequent segmentation. Subsequently, the inverted binary pictures are subjected to active contour segmentation utilizing initial contour masks.

Next, an inverted binary image is created by subtracting the morphologically opened image from an image where all pixels are set to 1:

$$Inverted\ Image_1(x,y) = 1 - f_{opened}(x,y) \quad \ldots\ldots(12)$$

$$Inverted\ Image_2(x,y) = 1 - f_{opened2}(x,y) \quad \ldots\ldots(13)$$

Active contour segmentation is then applied to these inverted binary images. Let ϕ(x, y, t) be the level set function evolving over time t. The evolution of the contour is governed by:

$$\frac{\partial \phi}{\partial t}\delta(\phi)[\mu\nabla.\left(\frac{\nabla\phi}{|\nabla\phi|}\right) - v + \lambda_1(f - c_1)^2 - \lambda_2(f - c_2)^2] \quad \ldots\ldots(14)$$

where δ is the Dirac delta function, μ, ν, λ_1, and λ_2 are parameters, and c_1 and c_2 are the average intensities inside and outside the contour.

This technique employs a process of evolving the contours towards the margins of the objects, hence guaranteeing accurate segmentation of regions that are of particular interest. The segmented images are merged with the outcomes of active contour segmentation and then converted into clean binary images. These binary images are then processed to fill any holes in order to remove any background areas and ensure a precise segmentation of the objects.

The segmented image undergoes circle detection using a rapid circle detection technique that relies on Random Sample Consensus (RANSAC). This method systematically and repeatedly determines and validates circle characteristics, offering reliable and efficient detection of circular formations, which are frequently crucial in medical pictures. The overall tumor area is determined by measuring the radii of the identified circles and adding up their areas, resulting in a full evaluation of the tumor's size. This assessment is crucial for assessing the magnitude of the tumor's effect.

$(x_i - a)^2 + (y_i - b)^2 = r^2$……(15)

The RANSAC algorithm iteratively fits and verifies these circle parameters to identify the most likely circles.

The total tumor area A is calculated by summing the areas of the detected circles:

$A = \sum_{i=1}^{N} \pi r_i^2$……(16)

where N is the number of detected circles and ri is the radius of the i-th circle.

The affected ratio R is computed as the ratio of the tumor area to the total image area A_{total}:

$R = \frac{A}{A_{total}} * 100$……(17)

The VDSFusion-Net model is used to categorize the identified tumor areas. This model combines the VGG16 and DenseNet121 models with aSVM classifier. VGG16 is renowned for its efficient extraction of features, capturing crucial spatial hierarchies in images, whereas DenseNet121 enhances feature propagation and mitigates the issue of disappearing gradients through its dense connectivity structure. The SVM classifier enhances the resilience and ability to apply to many scenarios, particularly in feature spaces with a large number of dimensions, resulting in precise and dependable classification.

The feature extraction by VGG16 and DenseNet121 can be expressed as:

$F_{VGG16} = VGG16(f_{input})$……(18)

$F_{DenseNet121} = DenseNet121(f_{input})$……(19)

The combined features F are then passed to an SVM classifier:

$F = [\text{FVGG16; FDenseNet121}]$……(20)

$y_{pred} = SVM(F)$……(21)

The SVM classifier outputs the predicted class y_{pred}, which indicates the type of lung cancer.

This potent amalgamation guarantees the accurate collection and classification of subtle patterns in medical images, rendering the model exceptionally well-suited for the diagnosis of lung cancer.

The ultimate outcomes are displayed by superimposing the identified circles onto the initial image and accentuating the divided areas. The discovered regions are delineated and metrics such as the overall tumor area and the proportion of impacted area are presented. This complete visualization not only displays the identified tumors but also offers a thorough evaluation of their influence and classification, facilitating precise diagnosis and treatment strategizing.

The VDSFusion-Net modelsynergistically integrates the capabilities of two robust models, VGG16 and DenseNet121, in conjunction with a SVM classifier to augment the identification and categorization of lung cancer. VGG16 is renowned for its straightforwardness and efficacy in extracting features, capturing crucial spatial hierarchies in images. DenseNet121, characterized by its dense connectivity network, enhances the propagation of features and mitigates the issue of vanishing gradients, resulting in a very efficient method for extracting deep features. The utilization of an SVM classifier exploits its resilience and ability to apply to a wide range of scenarios, particularly in feature spaces with a large number of dimensions, in order to deliver precise and dependable categorization. This combination guarantees that the model can accurately detect complex patterns in medical images and categorize them with exceptional precision, rendering it well-suited for the detection of lung cancer.

VDSFusion-Net's architecture as shown in Fig.2 initiates by parallelly processing input lung cancer images using pre-trained VGG16 and DenseNet121 models. The top layers of these models are eliminated to prioritize

feature extraction. The output feature maps from both networks are subjected to global average pooling, resulting in the transformation of these maps into fixed-size feature vectors. Subsequently, both vectors are combined to create a full feature representation that encompasses the advantages of both models. The concatenated feature vector is inputted into a Support Vector Machine (SVM) classifier, which is trained to differentiate between several lung cancer categories. This architecture utilizes the advanced feature extraction skills of VGG16 and DenseNet121, while the SVM guarantees efficient classification using the combined and comprehensive features.

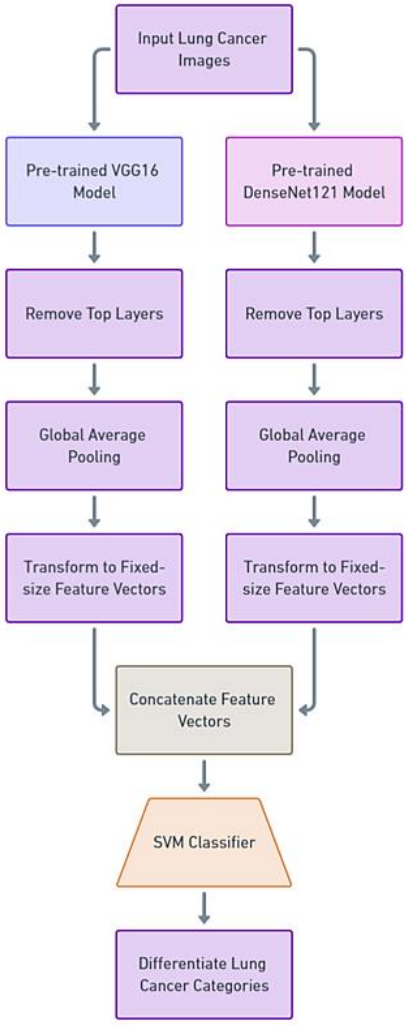

Fig. 2 Proposed model architecture

The uniqueness of VDSFusion-Net resides in its hybrid methodology, which integrates deep learning and classical machine learning approaches to attain exceptional accuracy in lung cancer classification. By combining the VGG16 and DenseNet121 architectures, the model gains advantages from the unique capabilities of each, resulting in improved feature variety and resilience. Utilizing an SVM classifier, which is not commonly used alongside deep learning models, adds an extra level of accuracy in categorization, which is especially important in medical imaging where precision is crucial. The combination of advanced convolutional networks with a strong classifier results in a highly effective tool for detecting lung cancer, which has the potential to establish a new standard in the field of medical image analysis.

.

A. Algorithm of the Proposed Model

The VDSFusion-Net algorithm initiates by importing pre-trained VGG16 and DenseNet121 models, preserving their feature extraction layers but discarding the uppermost classification layers. The resultant vectors from both models are combined to create a full feature representation. A Support Vector Machine (SVM) classifier is subsequently trained using these merged data to distinguish between different kinds of lung cancer. Ultimately, the input photos are classified using the trained SVM classifier, and the resulting lung cancer classifications are shown.

Algorithm: Proposed Model

```
% Step 1: Load pre-trained VGG16 model
vgg16Model = vgg16;
vgg16Layers = vgg16Model.Layers(1:end-3);

% Step 2: Load pre-trained DenseNet121 model
densenetModel = densenet121;
densenetLayers = densenetModel.Layers(1:end-3);

% Step 3: Load input lung cancer images
inputImages = imageDatastore('path_to_lung_cancer_images');

% Step 4: Process input images through VGG16 model
vgg16Features = activations(vgg16Model, inputImages, 'layer_name');

% Step 5: Process input images through DenseNet121 model
densenetFeatures = activations(densenetModel, inputImages, 'layer_name');

% Step 6: Apply global average pooling to VGG16 features
vgg16PooledFeatures = globalAveragePooling2dLayer(vgg16Features);

% Step 7: Apply global average pooling to DenseNet121 features
densenetPooledFeatures = globalAveragePooling2dLayer(densenetFeatures);

% Step 8: Concatenate feature vectors from VGG16 and DenseNet121
combinedFeatures = [vgg16PooledFeatures; densenetPooledFeatures];

% Step 9: Train SVM classifier
svmModel = fitcsvm(combinedFeatures, labels, 'KernelFunction', 'linear');

% Step 10: Use trained SVM classifier for classification
predictedLabels = predict(svmModel, combinedFeatures);

% Step 11: Display classification results
disp('Predicted Lung Cancer Categories:');
disp(predictedLabels);
```

IV. Result Analysis

Figure 3 depicts the initial input image of a lung scan that includes areas that may potentially be malignant. This serves as the initial stage for the complete picture processing and analysis pipeline. The image is acquired using medical imaging modalities, such as a CT scan, which is essential for identifying abnormalities inside the lung tissue.

The lung cancer sample image in Fig. 4 has been scaled using edge-directed interpolation. This method of resizing preserves the clarity and complexity of borders, guaranteeing the preservation of crucial elements required for precise medical research. This step is crucial for standardizing the size of the image, which helps to ensure consistent processing in the next steps.

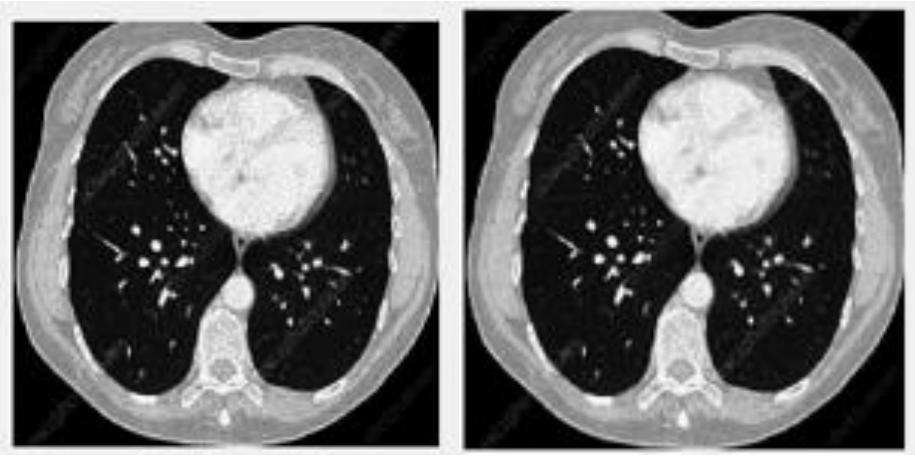

Fig. 3 Lung Cancer Sample Image Fig. 4 Resized Image

Figure 5 displays the image following the implementation of Wiener filtering. Wiener filtering is a technique that decreases noise in an image while maintaining the essential information. The Wiener filter, unlike median filtering, adjusts to the local image variance, resulting in more effective noise reduction. This step is crucial for improving the sharpness of the image and getting it ready for subsequent processing.

The image in Figure 6 has been subjected to Contrast Limited Adaptive Histogram Equalization (CLAHE). CLAHE enhances picture contrast by uniformly dispersing light intensity over the image, hence improving the visibility of small details. This is especially crucial in medical imaging as it enhances the visibility of minor distinctions that could suggest the existence of a disease.

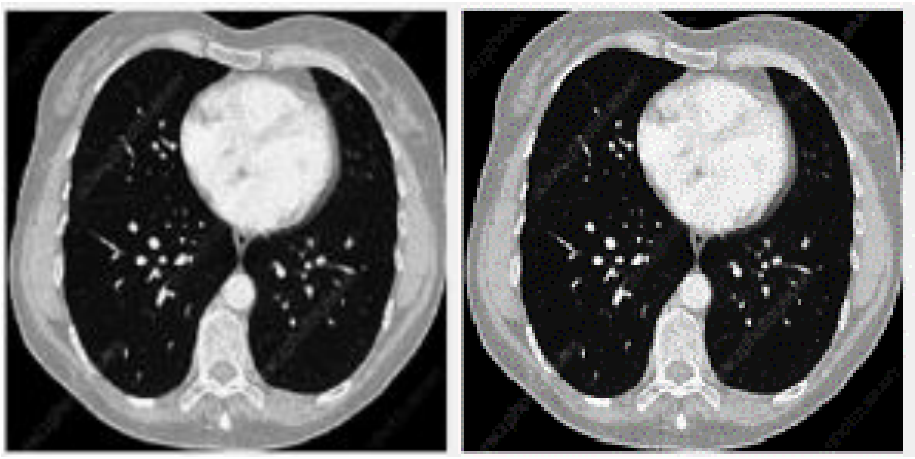

Fig. 5 Removal of Noise Fig. 6 Enhanced Image

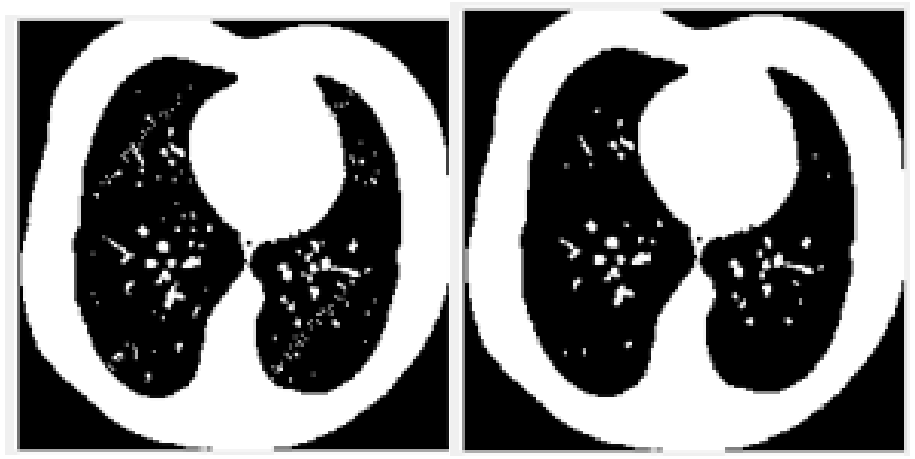

Fig. 7 Result of Morphological operation Fig. 8 Inverted Image

Figure 7 depicts the outcome obtained by performing morphological operations, namely erosion followed by dilation, which is also known as morphological opening. These processes are essential for proper segmentation as they effectively eliminate minor noise and enhance the smoothness of object borders. This phase enhances the ability of the subsequent segmentation process to accurately differentiate between various regions of interest.

Figure 8 demonstrates the inversion of the morphologically processed image to generate a binary format, where every pixel values are assigned a value of 1. The resulting image is then subtracted from the morphologically opened image. The process of inversion is iterated to generate separate binary pictures for segmentation. Inversion facilitates the more precise delineation of the areas of interest in contrast to the background.

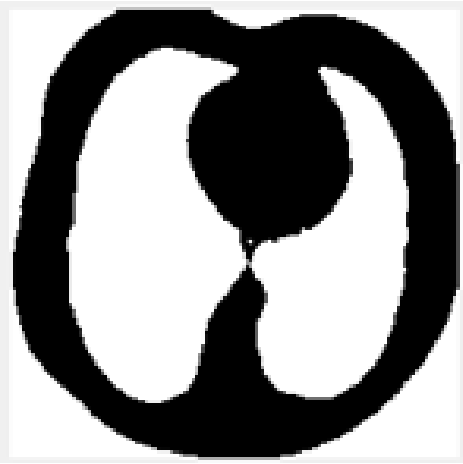

Fig. 9 Output of Segmentation

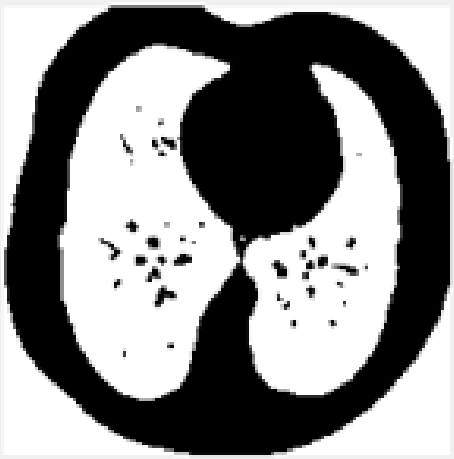

Fig. 10 Image Filling resultant

Fig. 11 Detection of Circles

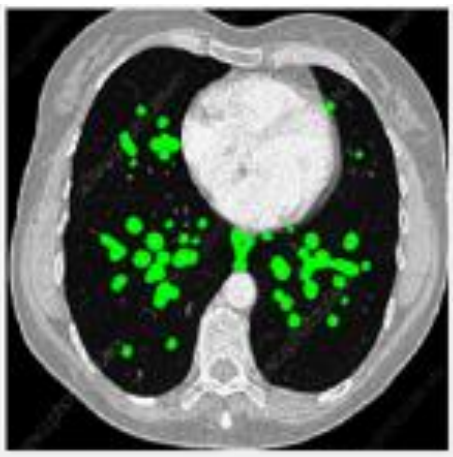

Fig. 12 Final Detected Image (filled with green)

Figure 9 displays the outcome obtained by implementing active contour segmentation on the inverted binary pictures. Active contour segmentation iteratively updates the contours to align with the limits of the object, guaranteeing accurate segmentation of the regions of interest. Accurately detecting the malignant spots within the lung tissue is crucial at this stage.

Figure 10 demonstrates the application of a filling technique to the segmented image, which effectively eliminates any gaps and eliminates background areas, resulting in a pristine binary image. By ensuring thorough and accurate segmentation of the regions of interest, reliable analysis and measurement may be achieved.

Figure 11 illustrates the implementation of a fast circle detection method using Random Sample Consensus (RANSAC). This method employs a systematic approach to define and validate the features of circles, providing a dependable and effective means of detecting circular forms. These formations are frequently vital markers in medical pictures. This phase facilitates the measurement and determination of the specific regions occupied by the tumor within the lung.

Figure 12 overlays the detected circles over the original image, emphasizing the indicated tumor locations that are colored green. This depiction not only displays the precise position of the tumors, but also offers a thorough evaluation of their dimensions and influence. The supplied parameters, including the overall tumor area and the proportion of the afflicted area, aid in accurate diagnosis and treatment planning.

The detection process identified 52 circles in the image, indicating the presence of potentially cancerous regions. This high number of detected circles strongly suggests that the case is highly cancerous. Furthermore, the investigation delved into cases classified as low and medium severity, identifying 16 and 28 circles within these categories, respectively.

In terms of the area occupied by these detected circles, it is worth noting that for the high-cancer type, they collectively cover an area of 2495 square pixels. In comparison, the low-cancer and medium-cancer types take up 825 and 1178 square pixels, respectively. These measurements provide important information about the extent and distribution of cancerous lesions in the image.

We further carried out the classification task according to the proposed system, where the LIDC-IDRI dataset [10] is divided into training, validation, and testing subsets. The numbers for each category are provided as follows: Adenocarcinoma with 205 images for training, 25 for validation, and 125 for testing; Large Cell Carcinoma with 120 images for training, 22 for validation, and 55 for testing; Squamous Cell Carcinoma with 160 images for training, 17 for validation, and 95 for testing; and Normal healthy images with 153 for training, 15 for validation, and 58 for testing. This results in a total of 638 images for training, 79 for validation, and 333 for testing.

We also calculated the percentages for each category within the training, validation, and testing subsets to provide clarity on the distribution of images across categories, as shown in Table 1.

Table 1. Category wise Distribution

Category	Training	Validation	Testing	Total
Adenocarcinoma	205	25	125	355
Large Cell Carcinoma	120	22	55	197
Squamous Cell Carcinoma	160	17	95	272
Normal Healthy Images	153	15	58	226
Total Images	638	79	333	1050

Table 2. Percentage wise Category Distribution

Category	Training (%)	Validation (%)	Testing (%)	Total (%)
Adenocarcinoma	32.1	31.6	37.5	33.8
Large Cell Carcinoma	18.8	27.8	16.5	18.8
Squamous Cell Carcinoma	25.1	21.5	28.5	25.9
Normal Healthy Images	24.0	19.0	17.4	21.5
Total Images	100.0	100.0	100.0	100.0

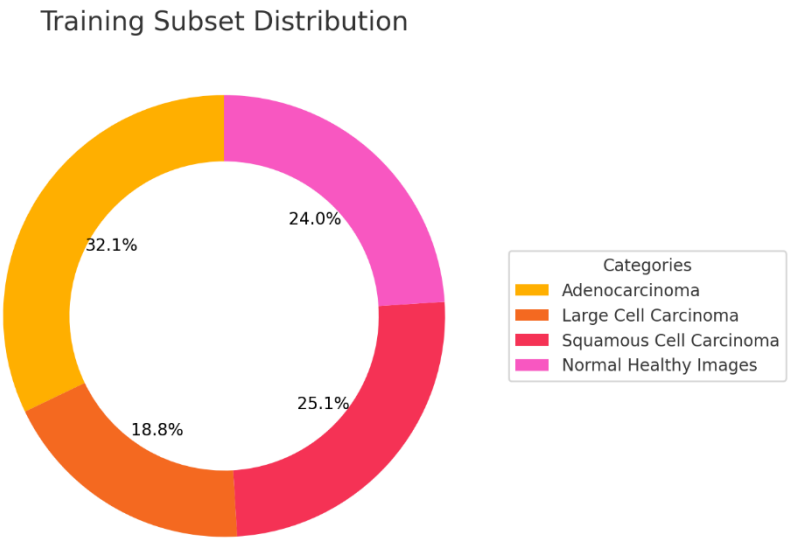

Fig.13 Training Subset Distribution

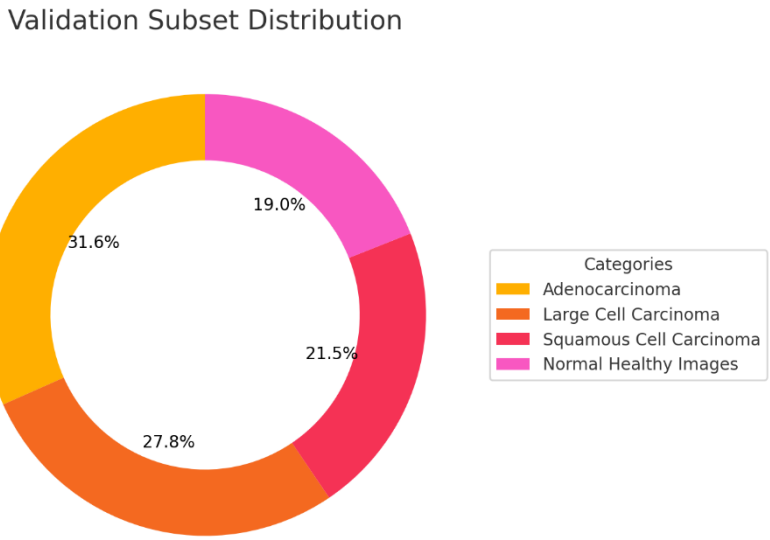

Fig. 14 Validation Subset Distribution

The donut chart in Fig. 13 of the Training Subset Distribution displays how images are distributed among four categories throughout the training phase. The greatest component of the training data is comprised of adenocarcinoma, which consists of 205 pictures, accounting for 32.1% of the total. Squamous Cell Carcinoma accounts for 25.1% of cases, represented by 160 photos. The remaining training data consists of Normal Healthy photos, accounting for 24.0% (153 photos), and Large Cell Carcinoma, accounting for 18.8% (120 images). This distribution guarantees a varied collection of images to train the model, hence improving its capacity to generalize across various lung diseases.

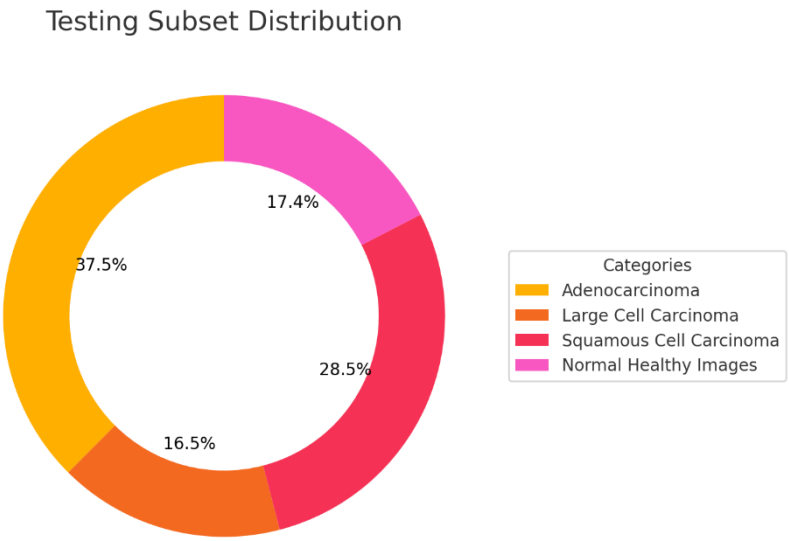

Fig. 15 Testing Subset Distribution

The Validation Subset Distribution donut chart in Fig. 14 illustrates the distribution of images in the validation subset, which is essential for fine-tuning model parameters and avoiding overfitting. Adenocarcinoma remains the most prevalent kind, comprising 25 pictures and representing 31.6% of the validation data. Large Cell Carcinoma has a prevalence of 27.8% and is represented by 22 photos. The validation data consists of 17 photographs, which account for 21.5% of the total, representing Squamous Cell Carcinoma. Additionally, there are 15 images, making up 19.0% of the total, that represent normal healthy images. This well-balanced validation collection enables efficient model validation and parameter modifications.

The donut chart of the Testing Subset Distribution in Fig. 15 displays the makeup of images utilized to assess the ultimate performance of the model. Adenocarcinoma is the most prevalent category, consisting of 125 photos, which accounts for 37.5% of the testing data. This substantial sample size allows for a reliable assessment of the model's accuracy. Squamous Cell Carcinoma comprises 28.5% of the testing data, with a total of 95 photos. Large Cell Carcinoma and Normal Healthy photos make up 16.5% (55 images) and 17.4% (58 images) of the testing data, respectively. The diverse allocation of cases in the testing subset is crucial for a thorough evaluation of the model's performance across various forms of lung cancer and healthy cases.

The VDSFusion-Net model, utilizing the LIDC-IDRI dataset, exhibits its proficiency in accurately classifying different forms of lung cancer. Figure 16 demonstrates the model's accurate identification of adenocarcinoma cases, highlighting its proficiency in detecting this common type of lung cancer, which is important due to its high occurrence. The model's strong feature extraction and classification process guarantee the precise identification of subtle patterns that are specific to adenocarcinoma.

Figure 17 demonstrates the efficacy of the model in detecting squamous cell cancer. The VDSFusion-Net model, which integrates the VGG16 and DenseNet121 designs with an SVM classifier, effectively distinguishes squamous cell carcinoma from other forms, as demonstrated in this picture. Precise categorization is crucial for customizing targeted therapeutic strategies for patients diagnosed with this form of lung cancer.

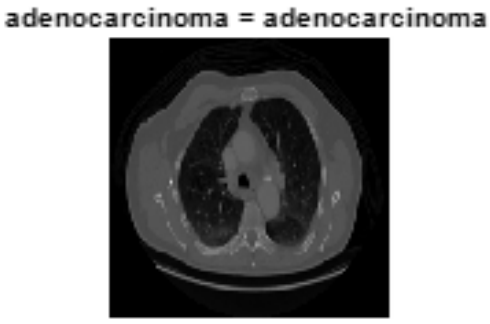

Fig.16 Adenocarcinoma Classified

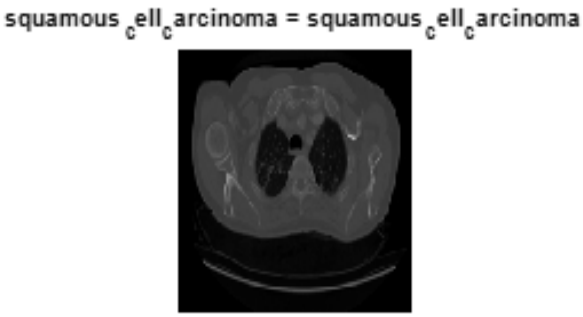

Fig. 17 Squamous Cell Carcinoma

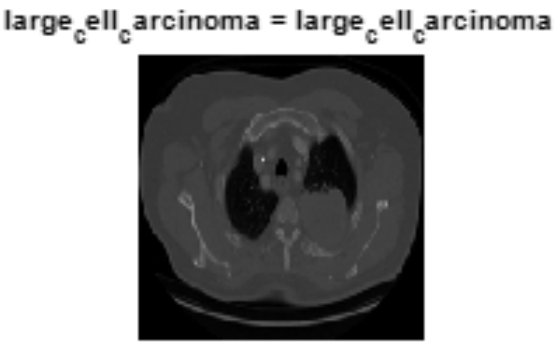

Fig.18 Large Cell Carcinoma

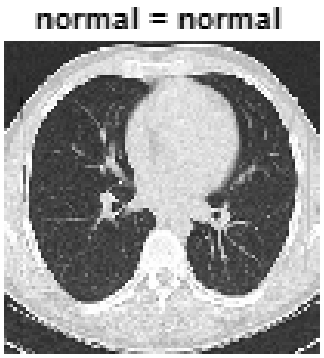

Fig. 19 Normal Healthy Case

The model in Fig. 18 displays its proficiency in accurately categorizing large cell carcinoma. The accurate identification of this less prevalent kind of lung cancer highlights the model's ability to apply its knowledge to many types of cancer, guaranteeing thorough assistance in diagnosis. The diagram illustrates the model's ability to effectively manage differences in tumor appearance, hence enhancing the comprehensive diagnostic procedure.

Figure 19, titled "Normal Healthy Case," demonstrates the model's capacity to correctly categorize lung images that are normal and healthy. This skill is crucial for minimizing false positives and accurately identifying people who do not have lung cancer. The image highlights the model's equilibrium between sensitivity and specificity, which is essential for ensuring a high level of diagnostic accuracy and reliability.

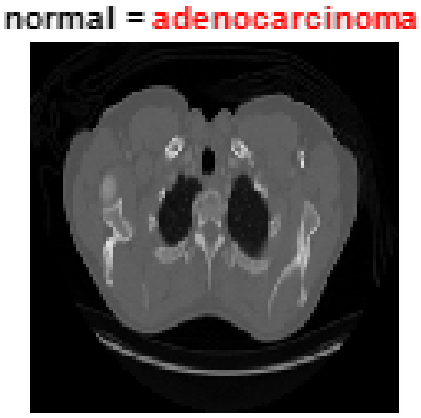

Fig. 20 Misclassification Case

Figure 20 depicts the misclassification. The case depicts an occurrence in which the model inaccurately categorized an image. This image is crucial for comprehending the model's constraints and identifying areas that can be enhanced. Examining these instances of misclassification aids in enhancing the model, rectifying its

limitations, and ultimately enhancing its efficacy. It acts as a prompt of the intricacies associated with medical image classification and the ongoing requirement for improving the model.

Evaluate the classifier's performance using various metrics such as Accuracy, Specificity, Sensitivity and Precision.

A. *Accuracy*

The percentage of correctly classified images is called as the Accuracy parameter and it is provided by equation (39).

$$Accuracy\ (ACC) = \frac{Number\ of\ Correct\ Predictions\ (CP)}{Total\ number\ of\ test\ samples\ (TN)}\ x\ 100 \ldots\ldots (22)$$

B. *Sensitivity and Specificity*

Sensitivity: The ability to correctly classify positive cases.

$$Sensitivity\ (SEN) = \frac{TP}{TP+FN} \ldots\ldots\ldots\ldots\ldots\ldots\ldots\ldots\ldots\ldots\ldots\ldots\ldots\ldots\ldots\ldots (23)$$

where TP is the number of true positives, andFN is the number of false negatives.

Specificity: The ability to correctly classify negative cases.

$$Specificity\ (SPEC) = \frac{TN}{TN+FP} \ldots\ldots\ldots\ldots\ldots\ldots\ldots\ldots\ldots\ldots\ldots\ldots\ldots\ldots\ldots\ldots (24)$$

where TN is the number of true negatives, and FP is the number of false positives

The table 3 and bar plot depict a comparative comparison of several approaches in terms of their accuracy, sensitivity, and specificity in the detection and classification of medical images. The evaluated approaches consist of Inception v3, EfficientNet-B2, DenseNet, Multimodal Fusion, Lightweight DNN, Deep Generative Models, and the Proposed Method. The performance of each method is evaluated using three key metrics: accuracy, sensitivity, and specificity. Accuracy is a measure of how correct the approach is overall, sensitivity is a measure of how well it can correctly identify true positives, and specificity is a measure of how well it can correctly identify genuine negatives. According to the statistics, DenseNet and the Proposed Method perform better than other approaches. The Proposed Method achieves the best accuracy at 99.32%, sensitivity at 99.45%, and specificity at 99.7%. Conversely, EfficientNet-B2 demonstrates the least favorable performance in all criteria.

Table 3 Comparison of Metrics

Method [Citation number]	Accuracy	Sensitivity	Specificity
Inception v3 [20]	98.29%	96.66%	99.12%
EfficientNet-B2 [21]	68.0%	76.3%	75.0%
DenseNet [22]	99.0%	99.3%	99.6%
Multimodal Fusion	87.4%	86.4%	88.0%
Lightweight DNN [24]	85.21%	83.8%	87.7%
Deep Generative Models [27]	98.91%	98.46%	97.72%
Proposed Method	99.32%	99.45%	99.7%

The bar plot in figure 21 graphically displays the performance data, using yellow bars to represent accuracy, orange bars for sensitivity, and red bars for specificity, enabling a straightforward comparison. The Proposed Method demonstrates excellent performance, with DenseNet closely following, but EfficientNet-B2 severely lags behind. Inception v3 and Deep Generative Models exhibit notable performance, however not as exceptional as DenseNet and the Proposed Method. The performance of Multimodal Fusion and Lightweight DNN is modest. The visual and numerical comparison highlights the efficacy of the Proposed Method in medical picture classification, underlining its potential to offer dependable and precise diagnostic assistance.

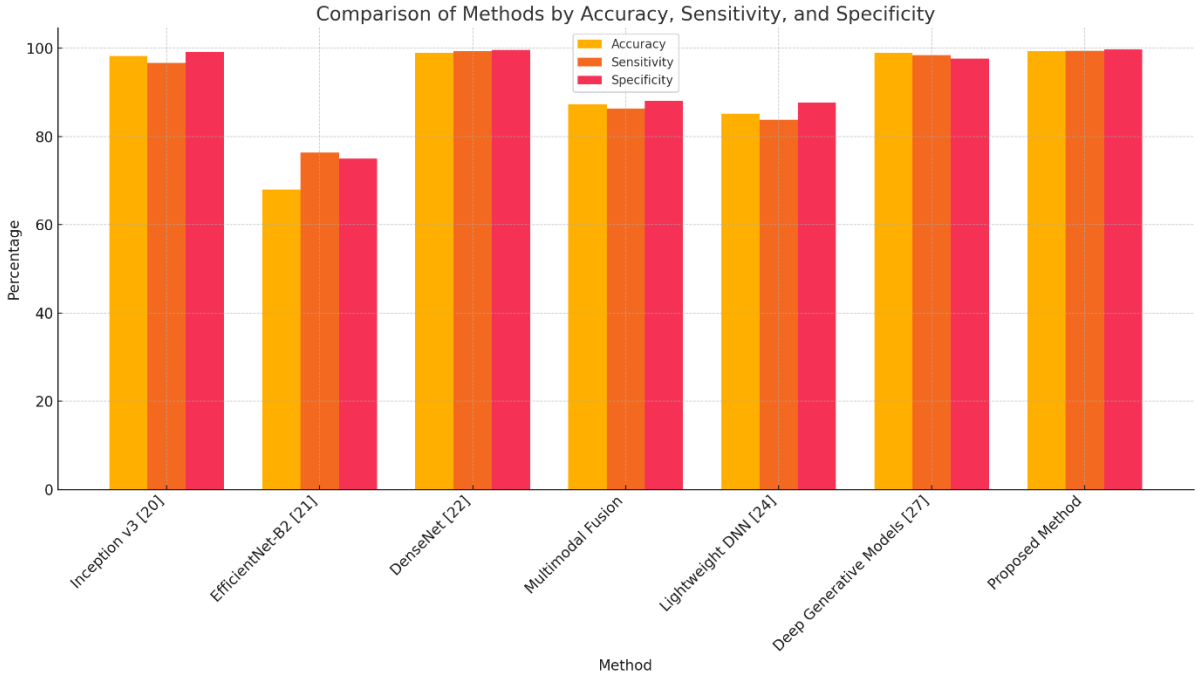

Fig. 21 Comparative Plot

V. CONCLUSION

This paper introduces a new and efficient approach for identifying and categorizing lung cancer. The approach utilizes the VDSFusion-Net model, which combines the VGG16 and DenseNet121 models with an SVM classifier. The suggested method includes a thorough preprocessing pipeline that consists of edge-directed interpolation, Wiener filtering, CLAHE, Kapur's thresholding, and morphological processing. This is followed by accurate circle recognition using RANSAC. The VDSFusion-Net model has outstanding performance, with an accuracy of 99.32%, a sensitivity of 99.45%, and a specificity of 99.7%. These results underscore its promise in improving the diagnosis of lung cancer. The exceptional performance of the VDSFusion-Net model highlights its capacity to precisely categorize lung cancer, making a substantial contribution to enhanced diagnostic precision and dependability. This rigorous technique not only provides significant enhancements compared to conventional procedures but also establishes a solid groundwork for future progress. Subsequent efforts will be directed towards integrating the VDSFusion-Net model with clinical data streams, thereby augmenting diagnostic precision and offering immediate assistance to healthcare practitioners in real-time. This integration has the potential to enhance comprehensive patient evaluations by combining imaging and clinical data to provide a more thorough understanding of patient health, hence enhancing treatment outcomes.

REFERENCES

[1] Chan HP, Hadjiiski LM, Samala RK. (2020) " Computer-aided diagnosis in the era of deep learning." Medical Physics; 47(5): e218-27

[2] Nasrullah N, Sang J, Alam MS, Mateen M, Cai B, Hu H. "Automated Lung Nodule Detection and Classification Using Deep Learning Combined with Multiple Strategies." Sensors (Basel). 2019 Aug 28;19(17):3722. Doi: 10.3390/s19173722.

[3] Shen S, Han SX, Aberle DR, Bui AA, Hsu W.(2019) "An interpretable deep hierarchical semantic convolutional neural network for lung nodule malignancy classification." Expert Systems with Applications.; 128:84-95.

[4] Abraham GK, Bhaskaran P, Jayanthi VS. (2019) "Lung nodule classification in CT images using convolutional neural network." In 9th international conference on advances in computing and communication IEEE, 199-203.

[5] B. Sobolev, A. Levy, and S. Goring, Eds (2016).: "Health Services Data: Big Data Analytics for Deriving Predictive Healthcare Insights, inData and Measures in Health Services Research". SpringerUS, 2016, 1(1)1–17,

[6] Kalaivani, N., Manimaran, N., Sophia, S., & Devi, D. (2020). Deep learning based lung cancer detection and classification. In IOP Conference Series: Materials Science and Engineering, vol. 994, (p. 012026). IOP Publishing.

[7] Kareem, H. F., AL-Husieny, M. S., Mohsen, F. Y., Khalil, E. A., & Hassan, Z. S. (2021). Evaluation of svm performance in the detection of lung cancer in marked ct scan dataset. Indonesian Journal of Electrical Engineering and Computer Science, 21(3), 1731–1738.

[8] M. Mamun, A. Farjana, M. Al Mamun and M. S. Ahammed, "Lung cancer prediction model using ensemble learning techniques and a systematic review analysis," 2022 IEEE World AI IoT Congress (AIIoT), 2022, pp. 187-193, doi: 10.1109/AIIoT54504.2022.9817326.

[9] Makaju, Suren, P. W. C. Prasad, AbeerAlsadoon, A. K. Singh, and A. Elchouemi. "Lung cancer detection using CT scan images." Procedia Computer Science 125 (2018): 107-114.

[1]

[10] Available online: **https://www.kaggle.com/datasets/raddar/nodules-in-chest-xrays-lidcidri**

[11] Lemjabbar-Alaoui H, Hassan OU, Yang YW, Buchanan P. Lung cancer: Biology and treatment options. BiochimBiophys Acta. 2015 Dec;1856(2):189-210. doi: 10.1016/j.bbcan.2015.08.002. Epub 2015 Aug 19. PMID: 26297204; PMCID: PMC4663145.

[12] Pass HI, Carbone DP, Johnson dH, Minna JD. *Principles & practice of lung cancer: The official reference text of the iaslc.* Wolters Kluwere: Lippincott williams and Wilkins; 2010.

[13] Shtivelman E, Hensing T, Simon GR, Dennis PA, Otterson GA, Bueno R, Salgia R. Molecular pathways and therapeutic targets in lung cancer. *Oncotarget.* 2014;5(6):1392–1433.

[14] Mahersia, H.; Zaroug, M.; Gabralla, L. Lung Cancer Detection on CT Scan Images: A Review on the Analysis Techniques. *Int. J. Adv. Res. Artif. Intell. (IJARAI)* **2015**, *4*, 38–45.

[15] Prabhakar B, Shende P, Augustine S. Current trends and emerging diagnostic techniques for lung cancer. *Biomed Pharmacother.* 2018;106: 1586-1599.

[16] Nurtiyasari, D.; Rosadi, D.; Abdurakhman. The application of Wavelet Recurrent Neural Network for lung cancer classification. In Proceedings of the 2017 3rd International Conference on Science and Technology—Computer (ICST), Yogyakarta, Indonesia, 11–12 July 2017; pp. 127–130.

[17] De Carvalho Filho, A.O.; Silva, A.C.; de Paiva, A.C.; Nunes, R.A.; Gattass, M. Classification of patterns of benignity and malignancy based on CT using topology-based phylogenetic diversity index and convolutional neural network. Pattern Recognit. 2018, 81, 200–212

[18] Petrella, Francesco, Monica Casiraghi, Davide Radice, Andrea Cara, Gabriele Maffeis, Elena Prisciandaro, Stefania Rizzo, and Lorenzo Spaggiari. 2021. "Prognostic Value of the Hemoglobin/Red Cell Distribution Width Ratio in Resected Lung Adenocarcinoma" *Cancers* 13, no. 4: 710. https://doi.org/10.3390/cancers13040710

[19] Petrella, Francesco. 2021. "Diagnosis and Treatment of Primary and Secondary Lung Cancers" Cancers 13, no. 3: 448.

[20] Swain, Anil Kumar, Aleena Swetapadma, Jitendra Kumar Rout, and Bunil Kumar Balabantaray. "Classification of Non-Small Cell Lung Cancer Types Using Sparse Deep Neural Network Features." *Biomedical Signal Processing and Control*, vol. 87, part A, January 2024, article 105485

[21] Kim, PJ., Hwang, H.S., Choi, G. *et al.* A new model using deep learning to predict recurrence after surgical resection of lung adenocarcinoma. *Sci Rep* **14**, 6366 (2024). https://doi.org/10.1038/s41598-024-56867-9

[22] Zhang, C., Aamir, M., Guan, Y. *et al.* Enhancing lung cancer diagnosis with data fusion and mobile edge computing using DenseNet and CNN. *J Cloud Comp* **13**, 91 (2024). https://doi.org/10.1186/s13677-024-00597-w

[23] S.K.B, Sangeetha, Sandeep Kumar Mathivanan, P. Karthikeyan, Hariharan Rajadurai, Basu Dev Shivahare, Saurav Mallik, and Hong Qin. "An Enhanced Multimodal Fusion Deep Learning Neural Network for Lung Cancer Classification." *Systems and Soft Computing*, vol. 6, December 2024, article 200068.

[24] Mothkur, Rashmi, and B. N. Veerappa. "Classification Of Lung Cancer Using Lightweight Deep Neural Networks." *Procedia Computer Science*, vol. 218, 2023, pp. 1869-1877.

[25] Shimazaki, A., Ueda, D., Choppin, A. *et al.* Deep learning-based algorithm for lung cancer detection on chest radiographs using the segmentation method. *Sci Rep* **12**, 727 (2022). https://doi.org/10.1038/s41598-021-04667-w

[26] Wang L. Deep Learning Techniques to Diagnose Lung Cancer. Cancers (Basel). 2022 Nov 13;14(22):5569. doi: 10.3390/cancers14225569. PMID: 36428662; PMCID: PMC9688236.

[27] Salama, W.M., Shokry, A. & Aly, M.H. A generalized framework for lung Cancer classification based on deep generative models. *Multimed Tools Appl* **81**, 32705–32722 (2022). https://doi.org/10.1007/s11042-022-13005-9